AGU PUBLICATIONS

JGR

Journal of Geophysical Research: Oceans

RESEARCH ARTICLE

10.1002/2016JC011948

Observed subseasonal variability of heat flux and the SST response of the tropical Indian Ocean

Sindu Raj Parampil[1,2], G. N. Bharathraj[1], Matthew Harrison[3], and Debasis Sengupta[1]

[1]Centre for Atmospheric and Oceanic Sciences, Indian Institute of Science, Bangalore, India, [2]Department of Earth Sciences, Uppsala University, Uppsala, Sweden, [3]Geophysical Fluid Dynamical Laboratory, Princeton, New Jersey, USA

Key Points:
- A satellite-based daily heat flux product created to study observed subseasonal variability in the tropical Indian Ocean
- Contribution of subseasonal changes in air-sea humidity gradients to latent heat flux equals the contribution of wind speed variations
- In the winter hemisphere, subseasonal SST variations are not a one-dimensional response to heat flux, but are mainly due to ocean processes

Supporting Information:
- Supporting Information S1

Correspondence to:
D. Sengupta,
dsen@caos.iisc.ernet.in

Citation:
Raj Parampil, S., G. N. Bharathraj, M. Harrison, and D. Sengupta (2016), Observed subseasonal variability of heat flux and the SST response of the tropical Indian Ocean, *J. Geophys. Res. Oceans*, *121*, 7290–7307, doi:10.1002/2016JC011948.

Received 9 MAY 2016
Accepted 7 SEP 2016
Accepted article online 9 SEP 2016
Published online 4 OCT 2016

Abstract We develop an experimental daily surface heat flux data set based on satellite observations to study subseasonal variability (periods shorter than 90 days) in the tropical Indian Ocean. We use incoming shortwave and longwave radiation from the International Satellite Cloud Climatology Project, and sea surface temperature (SST) from microwave sensors, to estimate net radiative flux. Latent and sensible heat fluxes are estimated from scatterometer winds and near-surface air temperature and specific humidity from Atmospheric Infrared Sounder (AIRS) observations calibrated to buoy data. Seasonal biases in net heat flux are generally within 10 W m^{-2} of estimates from moorings, and the phases and amplitudes of subseasonal variability of heat fluxes are realistic. We find that the contribution of subseasonal changes in air-sea humidity gradients to latent heat flux equals or exceeds the contribution of subseasonal changes in wind speed in all seasons. SST responds coherently to subseasonal oscillations of net heat flux associated with active and suppressed phases of atmospheric convection in the summer hemisphere. Thus, subseasonal SST changes are mainly forced by heat flux in the northeast Indian Ocean in northern summer, and in the 15°S–5°N latitude belt in southern summer. In the winter hemisphere, subseasonal SST changes are not a one-dimensional response to heat flux, implying that they are mainly due to oceanic advection, entrainment, or vertical mixing. The coherent evolution of subseasonal SST variability and surface heat flux suggests active coupling between SST and large-scale, organized tropical convection in the summer season.

1. Introduction

On intraseasonal time scales (30–90 day periods), the prominent modes of atmospheric variability in the tropical Indian Ocean are the northward moving monsoon ISO (MISO) in boreal summer (May–October) and the eastward moving Madden-Julian Oscillation (MJO). MJO is present through the year, but its amplitude is largest in boreal winter (November–April). Over the life cycle of MISO or MJO, tropical Indian Ocean SST cools during periods of active atmospheric convection with low incident sunlight and strong winds, and warms during suppressed convection when the sky is clear and winds are calm [*Lau and Waliser*, 2012]. The SST response to MISO extends from the Arabian Sea to the west Pacific, with the most energetic SST variability in the Bay of Bengal and South China Sea [*Bellenger and Duvel*, 2007; *Duvel and Vialard*, 2007]. The SST response to MJO is most prominent in the equatorial Indian Ocean (IO) south of the equator. During the active phase of MISO or MJO, SST cools because net heat flux at the ocean surface (Qnet) is negative, i.e., the ocean loses heat; in the suppressed phase of MISO or MJO, Qnet is positive and SST warms [e.g., *Shinoda et al*., 1998; *Sengupta and Ravichandran*, 2001; *Duvel and Vialard*, 2007]. Variability of atmospheric convection and SST on time scales shorter than 30 days also plays an important role in the Asian monsoon region [*Goswami*, 2012; *Lau and Waliser*, 2012]. For instance, *Han et al*. [2006] find that submonthly variability of Bay of Bengal SST (standard deviation ~0.2°C), which accounts for 30–50% of the total subseasonal variability, is forced mainly by surface heat flux.

Sengupta et al. [2001] showed from satellite observations that large-scale atmospheric deep convection, surface fluxes, and SST in the Bay of Bengal evolve in a coherent manner during summer, and proposed that the northward moving summer monsoon ISO is a coupled phenomenon, involving active air-sea interaction. The review by *Sobel et al*. [2010] concludes that feedback of surface fluxes is possibly the primary energy source for tropical intraseasonal variability. Modeling studies show stronger northward-propagating intraseasonal oscillations when the atmospheric model is forced by daily SST as opposed to monthly mean SST

in Atmospheric Model Intercomparison Project (AMIP) type runs. On the other hand, atmosphere-only models generally have weaker and less well-organized ISOs than coupled models [e.g., *Fu et al*., 2003; *Zheng et al*., 2004; *DeMott et al*., 2014; *Lau and Waliser*, 2012], indicating the importance of ocean-atmosphere feedback. Experiments using coupled air-sea models show that high-frequency, interactive Indian Ocean SST is a necessary condition for simulating the northward-propagating monsoon ISO, indicating the active role of SST in modulating MISO [e.g., *Achuthavarier and Krishnamurthy*, 2011; *Sharmila et al*., 2013]. *Sharmila et al*. [2013] also show that the coupled NCEP-Climate Forecast System with an interactive ocean produced northward propagation MISO while the same atmospheric model forced with daily SSTs from the coupled model output shows a dominant standing mode.

The contribution of ocean processes (advection, entrainment, and mixing) to subseasonal SST changes can be significant in some regions, but seasonally variable [e.g., *Schiller and Godfrey*, 2003; *Waliser et al*., 2004; *Vialard et al*., 2010]. The physics of subseasonal SST variability is an important open problem, because observations and models suggest that SST changes feedback on the organization and propagation of atmospheric convection in MJO and MISO, influencing the active-break cycles of the south Asian monsoon [e.g., *Sengupta et al*., 2001; *Vecchi and Harrison*, 2002; *Roxy and Tanimoto*, 2007; *Goswami*, 2012; *DeMott et al*., 2011]. Recent studies examine physical processes of ocean mixed layer depth (MLD) variations on intraseasonal time scales. *Schiller and Oke* [2015] use model output from an eddy-resolving OGCM to analyze MLD variability due to different terms in the temperature and salinity conservation equations. They find that MLD is influenced by heat and freshwater fluxes on intraseasonal time scales, particularly in the southern tropical Indian Ocean. *Halkides et al*. [2015] examine the spatial variability of the dominant processes of SST variability in the Indian Ocean. They find that apart from surface heat flux, subsurface ocean processes such as mixed layer deepening and shoaling can be important away from the equator, in particular near 8°S, 67°E in the Seychelles-Chagos Thermocline Ridge (SCTR) region. SST in the SCTR is sensitive to MLD variability because of the thin MLD, thin barrier layer and raised thermocline.

In the southern tropics, a marked SST response to passage of MJOs is seen in the eastern equatorial Indian Ocean and the SCTR in the southwest Indian Ocean (5°S–10°S, 60°E–90°E) [*Duvel and Vialard*, 2007]. *Xie et al*. [2002] showed that Ekman pumping due to large-scale wind stress curl raises the thermocline in the southwestern IO. *Zhou et al*. [2008] used model simulations to demonstrate that 40–80 day ocean Rossby waves generated by baroclinic instability propagate from the southeastern Indian Ocean to the west mainly in boreal winter and spring. Uncertainty in heat flux estimates on daily to weekly scales, and inadequate sampling of the upper ocean, may lead to uncertainty regarding the role of ocean processes in the mixed layer heat budget of this region.

During boreal winter (November–April) the thermocline and the upper mixed layer are shallow, and SST variability is largest in the SCTR. Intraseasonal variability of SST in the southern equatorial Indian Ocean is forced both by heat fluxes [*Duvel and Vialard*, 2007] and ocean processes [*Harrison and Vecchi*, 2001; *Vinayachandran and Saji*, 2008; *Saji et al*., 2006; *Lloyd and Vecchi*, 2010]. *Jayakumar et al*. [2010] use observations and an ocean model to study 30–90 day SST variability in the thermocline ridge during 1997–2006. They find that heat flux accounts for 70% of SST variability during several events of strong SST cooling; the contribution from wind stress is about 20%, where wind stress is a proxy for ocean processes. *Drushka et al*. [2012] used Argo data to analyze the heat budget of the ocean mixed layer in the region in response to MJO. They find that during the canonical MJO, mixed layer temperature variations are a response to net surface heat flux, mainly shortwave and latent heat flux anomalies. However, MJO-induced deepening and shoaling of the mixed layer depth can modulate the net heat flux and consequently the mixed layer temperature by as much as 40%.

In this study, we focus on the subseasonal variability of heat flux in the entire tropical Indian Ocean in all seasons. To better document and understand the subseasonal variability, we construct an experimental daily heat flux product based on observations, hereafter referred to as SatFlux. Available heat flux data fall into three main categories: (i) climatological or monthly mean atlases created from ship-based observations, such as the National Oceanography Centre (NOCS) [*Josey et al*., 1999] data set, (ii) atmospheric reanalyses such as those from the National Centers for Environmental Prediction-National Center for Atmospheric Research (NCEP-NCAR) [*Kalnay et al*., 1996] or the European Centre for Medium-Range Weather Forecasts (ECMWF), and (iii) satellite and reanalysis-based products (e.g., the Objectively Analyzed Air-Sea Heat Fluxes (OAFlux) [*Yu and Weller*, 2007]. Each class of flux data has its strengths and limitations: climatological atlases

give accurate estimates of air-sea parameters and heat fluxes but are mostly confined to shipping lanes. Reanalysis-based fluxes have good spatiotemporal coverage but are subject to model biases [*Yu et al.*, 2007]. Satellite data have good spatial coverage but are available for short periods (about 10 years in the case of daily data). Recent heat flux products such as OAFlux [*Yu and Weller*, 2007] and TropFlux [*Praveenkumar et al.*, 2011] incorporate surface meteorological data from all three sources to estimate daily fluxes. Both these data sets use shortwave radiation and net longwave radiation at the surface from the International Satellite Cloud Climatology Project (ISCCP) [*Zhang et al.*, 2004], and surface meteorological fields from in situ observations, satellites and reanalysis to estimate turbulent (latent and sensible) heat flux.

We construct an experimental daily surface heat flux data (SatFlux) for the period 2003–2007 for the tropical Indian Ocean (30°E–120°E, 30°S–30°N). Both radiative and turbulent fluxes are based purely on observations—we use daily satellite observations of SST and winds; daily satellite estimates of air temperature and humidity calibrated against buoy data; and a ship-based climatology to correct the seasonal cycle in surface air temperature and humidity. Using this heat flux data set, we aim to study (i) subseasonal variability (periods less than 90 days; ISV for brevity) of shortwave radiation, latent heat flux and net heat flux, (ii) impact of SST ISV and ISV of air temperature and humidity on latent heat flux, and (iii) the role of net heat flux ISV in forcing SST ISV.

SatFlux uses only satellite observations (apart from a ship-based climatology) and is the first heat flux product created using daily satellite air temperature (Ta) and humidity (Qa). Previously available daily heat flux products (e.g., OAFLUX and TropFlux) use surface meteorological parameters from model reanalyses like NCEP or data like CORE.2, which is based on NCEP reanalysis. Thus, the novelty of SatFlux lies in including the contribution of daily satellite Ta and Qa for studying the subseasonal variability in the monsoon region.

Section 2 has a more complete discussion of data and methods. In section 3, we briefly report validation and comparison with other flux products, and present our main results on the subseasonal variability of fluxes and their relation with SST. We summarize the main results and their implications in section 4.

2. Data and Methods

We use daily satellite data to construct net surface reaching shortwave radiation (Qsw) and net surface leaving longwave radiation (Qlw). Satellite and climatological data of air temperature and humidity are used to estimate latent heat flux (Qlat) and sensible heat flux (Qsens). So net surface heat flux, Qnet = Qsw + Qlw + Qlat + Qsens, where the positive sign stands for "into the ocean." Shortwave radiation penetrating below the mixed layer (Qpen), an important loss term in the mixed layer heat budget is also estimated. The residual of Qnet and Qpen is the amount of heat available for warming or cooling the mixed layer, we refer to this term as the "effective" heat flux Qeff.

2.1. Estimation of Radiative Fluxes: Qsw and Qlw

For estimating Qsw, the 3 hourly, 2.5° × 2.5° incoming shortwave radiation SW_{IN} from the International Satellite Cloud Climatology Project Flux Data (ISCCP-FD) [*Zhang et al.*, 2004] is averaged to daily values and interpolated onto a 1° × 1° grid. Net shortwave radiation Qsw = SW_{IN} (1 – 0.055) where the albedo of the ocean is taken to be 0.055. All satellite parameters are validated against data from the Research Moored Array for African-Asian-Australian Monsoon Analysis and Prediction (RAMA) [*McPhaden et al.*, 2009] in the Indian Ocean, and two buoys from the Tropical Atmosphere Ocean/Triangle Trans-Ocean Buoy Network (TAO) [*McPhaden et al.*, 1998] in the west Pacific Ocean. For example, we compared the 7 day smoothed Qsw from ISCCP to measurements from the RAMA mooring at 0°N, 90°E—the bias of the ISCCP Qsw (i.e., RAMA minus ISCCP) is 5 W m^{-2}; the correlation coefficient (Corr) between the two time series is 0.92 and the root-mean-square difference (RMSD) is 17 W m^{-2} (see Figure S1, supporting information). The bias and RMSD for all four RAMA locations are listed in Table 1.

ISCCP-FD incoming longwave radiation (LW_{IN}) also compares reasonably well with measurements at 0°N, 80.5°E. Outgoing longwave radiation (LW_{OUT}) at the surface is estimated from the Stefan-Boltzmann law:

$$LW_{OUT} = \varepsilon.\sigma.SST^4 \quad (1)$$

where ε is the emissivity of the sea surface and σ is the Stefan-Boltzmann constant; SST is in degree Kelvin. In the ISCCP data set, LW_{OUT} is calculated using equation (1) from satellite-derived ISCCP skin

Table 1. Bias and RMSD Between Estimated and In Situ Qsw at RAMA Locations

Location	Bias	Root-Mean-Square Difference
8°N, 90°E	−9	34
0°N, 90°E	5	18
1.5°S, 90°E	5	17
8°S, 67°E	0	61

SST and a frequency-dependent emissivity [*Rossow and Zhang*, 1995]; to estimate buoy LW_{OUT}, we use buoy SST and $\sigma = 0.98$ in equation (1). We find that ISCCP LW_{OUT} overestimates Buoy LW_{OUT} by 14 W m^{-2} (not shown). The difference arises mainly from errors in ISCCP skin SST, which has large subseasonal fluctuations (periods of 15–45 days), and can be 3–4 K higher than buoy SST (supporting information, Figure S2) or satellite SST from TMI-AMSRE [*Gentemann et al*., 2004] (W. Rossow, personal communication, 2005). Therefore, we use TMI-AMSRE SST in equation (1) to calculate LW_{OUT} over the tropical IO.

In equation (1), the sea surface is a gray body ($\varepsilon = 0.98$), so (1-ε). LW_{IN} accounts for the fraction of incoming longwave radiation reflected from the ocean surface. Hence, we estimate net surface longwave radiation (Qlw) as:

$$Qlw = -(LW_{OUT} - \varepsilon.LW_{IN}) \quad (2)$$

Our estimate of Qlw is compared with buoy estimates at 0°N, 165°E (TAO array) and 0°N, 80.5°E (RAMA; supporting information Figure S1b). The satellite estimate has a bias of 5.7 W m^{-2} at the RAMA location and RMSD of about 10 W m^{-2}. At 0°N, 165°E, the bias is 9 W m^{-2} and RMSD is 6 W m^{-2} (not shown).

2.2. Estimation of Turbulent Fluxes: Qlat and Qsens

Latent and sensible heat fluxes are estimated from satellite winds, air temperature (Ta), and specific humidity (Qa), together with TMI-AMSRE SST. Winds are from daily vector winds from the scatterometer on QuikSCAT [*Liu*, 2002] optimally interpolated onto a 1° × 1° grid [*Pegion et al*., 2000]. Ta and Qa are important variables in the calculation of turbulent fluxes, Qlat and Qsens. The Atmospheric Infrared Sounder (AIRS) onboard the Earth Orbiting system Aqua satellite, blended with microwave sounders on other satellites, provides daily vertical profiles of air temperature and humidity at 24 and 12 levels respectively, at 1° × 1° horizontal resolution [*Olsen et al*., 2007, 2013]: the AIRS level 3 data set has been made available at WMO standard pressure levels [*Olsen et al*., 2013]. The lowest three levels are 1000, 925, and 850 mb, i.e., a nominal vertical resolution of about 750 m in the lower atmosphere. We have not attempted to interpolate or extrapolate the observations to time-varying surface pressure. For simplicity, we take AIRS air temperature and humidity at 1000 mb to represent surface Ta and Qa. We note that the 1000 mb level always lies well within the atmospheric boundary layer, even in the winter hemisphere.

We first validate AIRS Ta and Qa using RAMA buoys from four locations in the Bay of Bengal along 90°E: 1.5°S, 0°N, 8°N, and 12°N. Qa at 1.5°S is available from 2003 to June 2004, while at all other locations, Qa is available from 2007. We find that AIRS Ta has a negative bias (bias = RAMA Ta − AIRS Ta), i.e., the satellite product underestimates air temperature; specific humidity is overestimated by satellite. Since the bias in AIRS Ta (+1.3 to +3.4°C) and Qa (−4.7%–0%) is substantial, we use the seasonal cycle (periods longer than 90 days) of Ta and Qa from the ship-based COADS climatology [*da Silva et al*., 1994] instead of the seasonal cycle from AIRS, but retain the subseasonal variability from AIRS (see below).

On subseasonal time scales, there is moderate correlation between AIRS and RAMA for both Qa (0.6) and Ta (0.4; see supporting information Figure S3). However, the magnitude of subseasonal variability of AIRS Ta is somewhat too high (supporting information Figure S3), perhaps because the 1000 hPa estimates are based on extrapolation from the 850 and 925 hPa values, where the air can be cooler relative to air at 10 m height. We therefore scale the subseasonal variability of satellite Ta using a constant correction factor of 0.8 (see below; supporting information Figure S3). It is important to note that AIRS Qa ISV needs no correction or scaling (supporting information Figure S3, bottom). Further, on intraseasonal scales AIRS Qa variability agrees significantly better with buoy Qa (Correlation 0.54) than reanalysis Qa from CORE-II (Correlation 0.3; supporting information Figure S4)

At each location, we define the correction factor as the ratio of the standard deviation of 2–90 day buoy data and 2–90 day AIRS data, i.e., $^{SD\ (2–90\ day\ Buoy)}/_{SD\ (2–90\ day\ AIRS)}$.

CF is the mean of the correction factors at all buoy locations, weighted by the number of data points at each location: we find that CF is 0.8 for Ta. So at each grid point,

$$Ta = Ta_{seasonal} + 0.8 \cdot Ta_{subseasonal} \quad (3)$$

Similarly,

$$Qa = Qa_{seasonal} + Qa_{subseasonal} \quad (4)$$

where $Ta_{seasonal}$ and $Qa_{seasonal}$ are Ta and Qa from da *Silva et al*. [1994] climatology.

$Ta_{subseasonal}$ and $Qa_{subseasonal}$ are the subseasonal component (2–90 days) of Ta and Qa from AIRS.

Using the calibrated Ta and Qa, QuikSCAT winds, and TMI-AMSRE SST, we calculate latent heat flux (Qlat) and sensible heat flux (Qsens) from bulk formulae according to *Zeng et al*. [1998]: $Qlat = -\rho_a.L_e.u_*.q_*$, where ρ_a is the density of air, L_e is latent heat of vaporization, and u_* and q_* are the friction velocity and humidity. The algorithm is based on Monin-Obukhov similarity, and the exchange coefficients are functions of surface wind speed and stability. We compare the satellite-based Qlat at 1.5°S, 90°S with in situ estimates of Qlat (i.e., Ta, Qa, winds, and SST are from the buoy). The bias is -9 W m^{-2} and RMSD is 20 W m^{-2}. Generally, satellite and buoy estimates compare reasonably well through the year, except for some occasions in summer (supporting information Figure S5). A possible reason is that AIRS Ta and Qa estimates are based on microwave as well as infrared radiances [*Olsen et al*., 2007], and the latter may not be accurate during cloudy monsoon conditions. We have compared standard deviations of 2–90 day variability of SatFlux Qlat with those of OAFLUX and TropFlux (supporting information Figure S6). Throughout the Indian Ocean region, SatFlux shows higher variability than OAFLUX and TropFlux.

2.3. Estimation of Penetrative Shortwave Radiation (Qpen)

Penetrative radiation below the mixed layer (Qpen) is estimated from satellite Qsw, SeaWIFS monthly chlorophyll *a* and climatological mixed layer depth [*de Boyer Montegut et al*., 2004] using the algorithm of *Morel and Antoine* [1994]. Chlorophyll *a*, a proxy for planktonic light absorption, determines the amount of sunlight that penetrates into the subsurface ocean. The attenuation depth (ζ), the depth at which shortwave radiation reduces to 1/e of its surface value, is about 15–20 m in the clear open waters of the eastern Arabian Sea and Bay of Bengal.

The mixed layer depth used in the Qpen calculation is the global, gridded monthly climatology from *de Boyer Montegut et al*. [2004]. MLD is estimated using a density criterion ($\rho_{mld} = \rho_{10m} + 0.03$ kg/m^3) from high vertical resolution individual density profiles from the National Oceanographic Data Center [*Conkright et al*., 2002] and the World Ocean Circulation Experiment database [*WOCE Data Products Committee*, 2002].

The general equation for the exponential decrease of shortwave radiation penetrating below the MLD follows *Morel and Antoine* [1994]

$$Qpen = Qsw.e^{-mld/\zeta} \quad (5)$$

Morel and Antoine [1994] provide an algorithm which accounts for upper ocean heating due to absorption of solar radiation by phytoplankton. Remotely sensed chlorophyll concentration is used to determine the vertical profile of radiation in the ocean: The infrared waveband is described by a single exponential function while the ultraviolet and visible bands are described by a bimodal exponential. Our choice of algorithm is based on validation against *in situ* subsurface sunlight from a field campaign during 23 May 2003 to 4 June 2003 [*Pradhan et al*., 2005]. A total of 106 profiles of subsurface sunlight were collected at 9.2°E, 74.5°N in the southeastern Arabian Sea from a multispectral radiometer (SATLANTIC Inc.), which measures downwelling radiation at seven discrete wavelengths in the 400–700 nm range. The measurements are extended to 300 nm and integrated over 300–700 nm. We compared daily averages of observed net downwelling shortwave radiation with estimates from the algorithms by *Paulson and Simpson* [1977], *Morel and Antoine* [1994], and *Manizza et al*. [2005] (supporting information Figure S7) at 10 and 30 m depths. At 10 m depth, *Morel and Antoine* [1994] compares best with observations (supporting information Figure S6a) while at 30 m depth, *Morel and Antoine* [1994] and *Manizza et al*. [2005] perform equally well (supporting information Figure S6b).

3. Results and Discussion

Figure 1 shows the 5 year mean (2003–2007) Qsw, Qlw, Qlat, and Qnet from SatFlux; basin averages of the heat flux components are mentioned in each plot. To place the SatFlux estimates in context, we compare

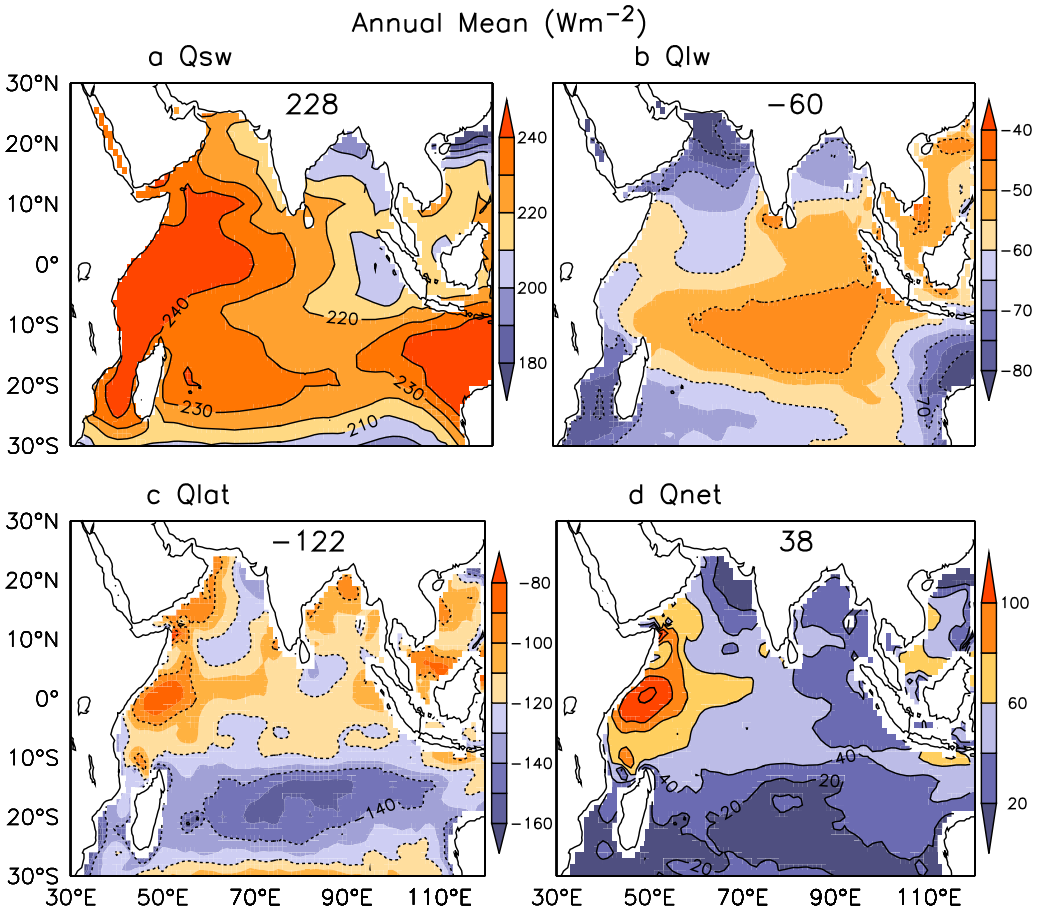

Figure 1. Five year (2003–2007) mean of SatFlux heat fluxes in W m^{-2}: (a) Qsw, (b) Qlw, (c) Qlat, and (d) Qnet. Basin-average values are mentioned in each plot. The contour intervals are: (a) Qsw, 10 W m^{-2}, (b) Qlw, 10 W m^{-2}, (c) Qlat, 20 W m^{-2}, and (d) Qnet, 20 W m^{-2}.

them with the National Oceanography Centre version 1 flux climatology (hereafter NOCS) [*Josey et al.*, 1999], and two daily heat flux data sets, namely the interannually varying Objectively Analyzed Air-sea Flux (OAFlux) [*Yu et al.*, 2007] and TropFLUX [*Praveenkumar et al.*, 2011] for the period 2003–2007.

3.1. Comparison of SatFlux With NOCS, OAFlux, and TropFLUX

The 5 year mean (2003–2007) basin average (30°E–120°E, 30°S–30°N) individual heat flux components Qsw, Qlw, and Qlat from SatFlux (Figure 1) all differ by less than 10 W m^{-2} from basin averages in the NOCS climatology: mean Qsw is 228 W m^{-2} in SatFlux and 221 W m^{-2} in NOCS (not shown). The main differences are in the north Bay of Bengal, where NOCS is about 20 W m^{-2} higher, and in the south western Indian Ocean where NOCS is about 20 W m^{-2} lower. SatFlux and NOCS Qlat have similar spatial patterns: Qlat is about −120 W m^{-2} in the Arabian Sea and −120 to −140 W m^{-2} in the southern Indian Ocean (IO). Basin-average Qlat is −122 W m^{-2} in SatFlux and −117 W m^{-2} in NOCS. Qlw is −51 W m^{-2} in NOCS and −60 W m^{-2} in SatFlux (not shown).

Basin-averaged 2003–2007 mean SatFlux Qnet is 38 W m^{-2}, while basin-averaged Qnet in the NOCS climatology is 46 W m^{-2} (Figure 2). The 2003–2007 mean basin-average SatFlux Qnet is 15 W m^{-2} higher than both 2003–2007 mean OAFlux and TropFLUX Qnet; note that SatFlux Qnet is higher throughout the basin (Figure 2). The main reason is that net longwave flux Qlw in OAFlux and TropFLUX is about 10–15 W m^{-2} higher than SatFlux Qlw. As discussed in section 2.2, OAFlux and TropFLUX directly use net longwave flux at the surface from ISCCP—the warm bias in ISCCP SST leads to higher outgoing longwave radiation in these two products.

On average, Qnet in the western equatorial Indian Ocean exceeds 80 W m^{-2} in all products. In the Bay of Bengal, SatFlux Qnet is 40 W m^{-2}, compared to 20–30 W m^{-2} in OAFLUX and TropFLUX, and 46 W m^{-2} in

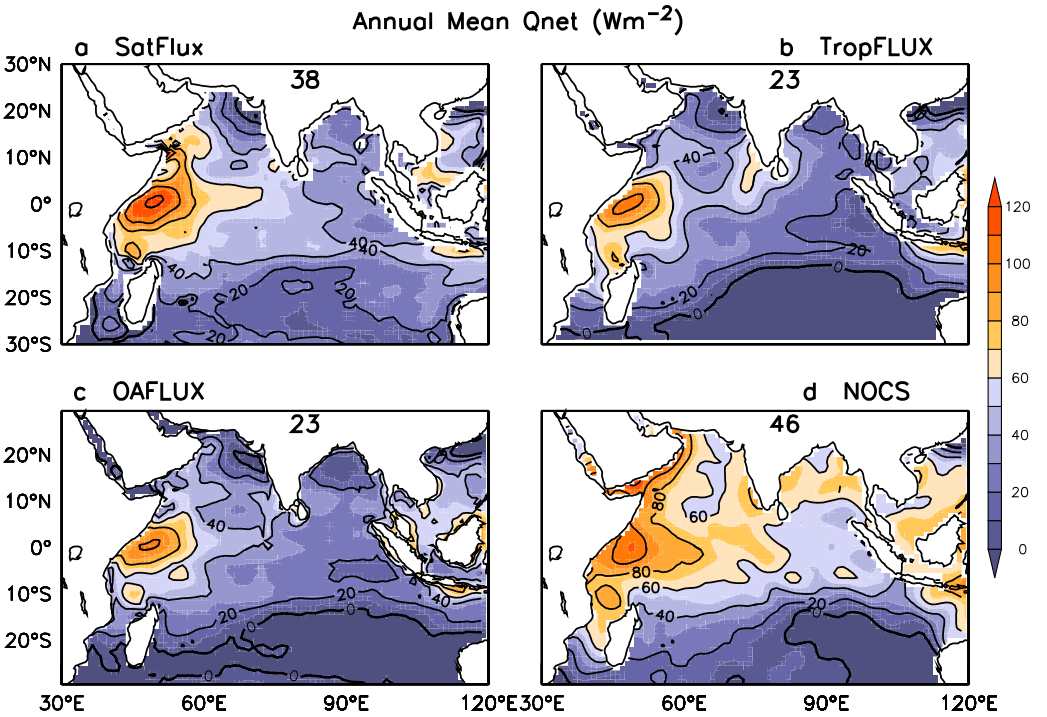

Figure 2. Five year mean (2003–2007) net surface heat flux Qnet (W m^{-2}) from daily (a) SatFlux, (b) TropFLUX, and (c) OAFlux data sets, and (d) Qnet from NOCS climatology.

the NOCS climatology. A notable difference between SatFlux and the other daily products is the absence of a region of heat loss (negative Qnet) in the southern Indian Ocean (Figure 2).

The 2003–2007 seasonal mean Qnet in February–May (FMAM) is greater than 40 W m^{-2} almost everywhere in the north Indian Ocean, with the equatorial western Indian Ocean gaining more than 80 W m^{-2} (Figure 3b). Much of the southern Indian Ocean south of 20°S loses heat during this period, except for the region off Australia. During the summer monsoon season June–September (JJAS), Qnet is positive everywhere north of 15°S; the basin average Qnet is about 11 W m^{-2} (Figure 3c). Even in the central Arabian Sea, where the monsoon wind speed can be 10–12 ms^{-1}, latent heat flux is low because air-sea humidity difference is small. Qsw is relatively low because the sky is often cloudy. The resultant Qnet is about 80 W m^{-2} in this region [*Weller et al.*, 1998], consistent with the NOCS climatology [*Josey et al.*, 1999]. During autumn and winter (ONDJ), the north Indian Ocean loses heat (Qnet is about −40 W m^{-2}), while there is net heat gain in other regions. The heat loss in the Arabian Sea and Bay of Bengal is generally attributed to high evaporation induced by cool, dry winds blowing off the continent [*Murtugudde and Busalacchi*, 1999; *Rao and Sivakumar*, 2003]. We note that subsidence over the central and southern Arabian Sea and Bay of Bengal is also a likely cause of dry surface air (see below). The largest Qnet is in the western Arabian Sea, due to high Qsw and relatively low Qlat.

Heat input to the upper mixed layer equals net surface heat flux minus penetrative flux of solar radiation through the mixed layer base. Annual mean penetrative radiation Qpen is 20–25 W m^{-2} in the northern Bay of Bengal and the equatorial Indian Ocean. Qpen varies significantly between seasons. In boreal summer (May–October, MJJASO), the sky is cloudy over much of the northern and equatorial Indian Ocean; surface wind speed in the summer monsoon season is enhanced not only in the north, but also in the southern hemisphere trade wind region. The cloudy skies and relatively deep mixed layers [*de Boyer Montegut et al.*, 2004] result in low Qpen nearly everywhere, with basin-average Qpen of about 9 W m^{-2} (Figure 4a). During November–April (NDJFMA), Qpen exceeds 20 W m^{-2} throughout the tropical Indian Ocean except in the Arabian Sea, and the basin average is 22 W m^{-2} (Figure 4b).

The effective heat flux available to the upper mixed layer ("Qeff") equals Qnet minus Qpen. The annual mean basin-average Qnet is equal to 38 W m^{-2}, Qpen is 16 W m^{-2}, and Qeff = 21 W m^{-2} (Figure 4c). The

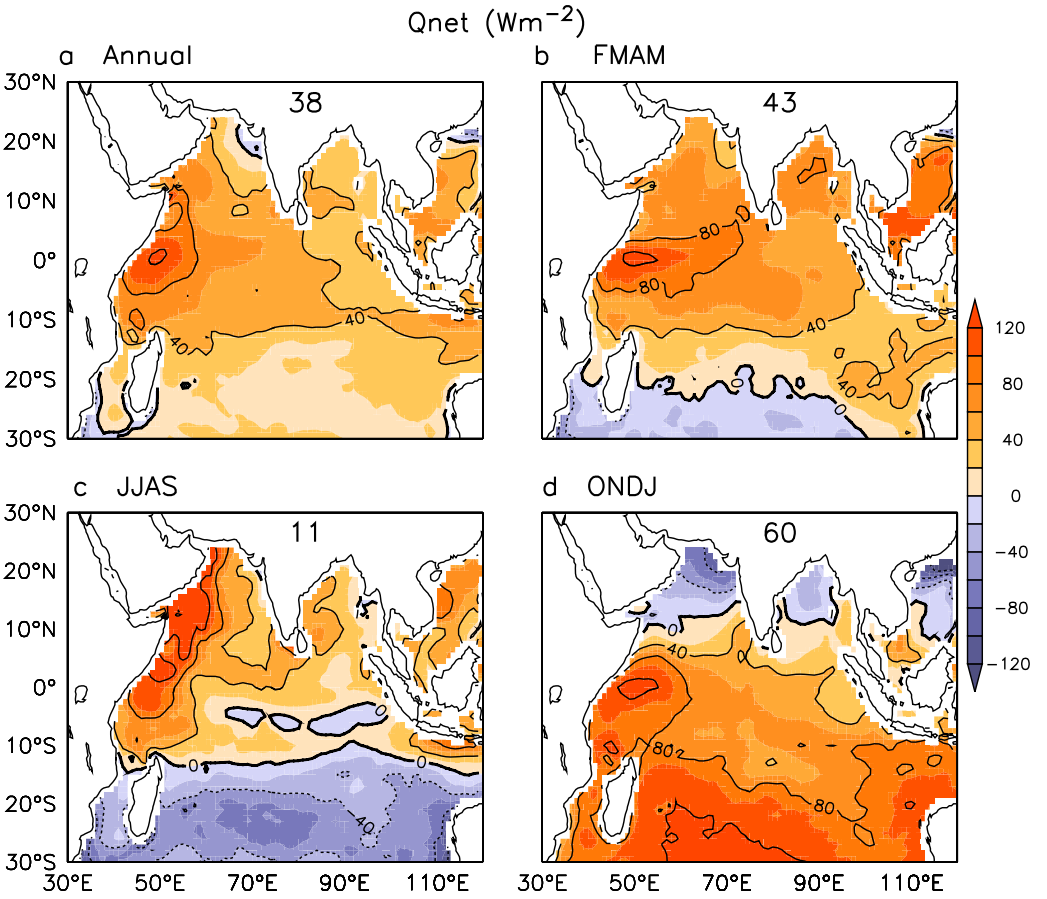

Figure 3. (a) Five year annual mean SatFlux Qnet (W m^{-2}). (b) As in Figure 3a but for February–May FMAM, (c) JJAS, and (d) ONDJ. Contour interval is 20 W m^{-2}.

spatial patterns of Qeff during the different seasons (Figures 4d–4f) are broadly similar to those of Qnet (Figure 3), but heat gain in the mixed layer is considerably smaller. The basin average Qeff is only 3 W m^{-2} in the summer monsoon season (June–September; JJAS) because the heat gain in the north Indian Ocean is nearly equal to heat loss south of about 15°S (Figure 4e). Note that there is net loss of heat from the mixed layer in the northern Arabian Sea and Bay of Bengal in October–January (ONDJ), but the basin average is 39 W m^{-2} because Qeff exceeds 60 W m^{-2} almost everywhere south of 10°S.

3.2. Subseasonal Variability of Fluxes

The subseasonal variability of net surface heat flux Qnet is highest in the boreal summer season, exceeding 80 W m^{-2} in the northeast Indian Ocean as well as in the central Indian Ocean south of 10°S (Figure 5). In other seasons, Qnet varies between 50 and 75 W m^{-2} in these regions (not shown). The large variability of Qnet in the northeast is due to the nearly in-phase fluctuations of Qsw and Qlat during the active-break cycles of the summer monsoon, with clear, calm conditions alternating with cloudy, windy phases [e.g., *Sengupta et al*., 2001]. The highest variability of shortwave radiation (60 W m^{-2}) is found in the Bay of Bengal (Figure 5a) [*Sobel et al*., 2010] and eastern equatorial Indian Ocean. The variability of Qsw is lowest to the south of 10°S, and in the western Arabian Sea, in particular the upwelling regions off Africa and the Arabian Peninsula (Figure 5a), where organized atmospheric convection is absent or very rare throughout the summer monsoon season.

The variability of Qlat is highest (50–70 W m^{-2}) south of 10°S, followed by the Arabian Sea and Bay of Bengal (Figure 5b). As mentioned earlier, the large Qnet ISV in the north IO is due to the superposition of Qsw and Qlat fluctuations. For example, the variability averaged over the Bay of Bengal is 54 W m^{-2} in Qsw and 48 W m^{-2} in Qlat, while the variability of net surface heat flux is 88 W m^{-2} (Figure 5d). The ISV of shortwave

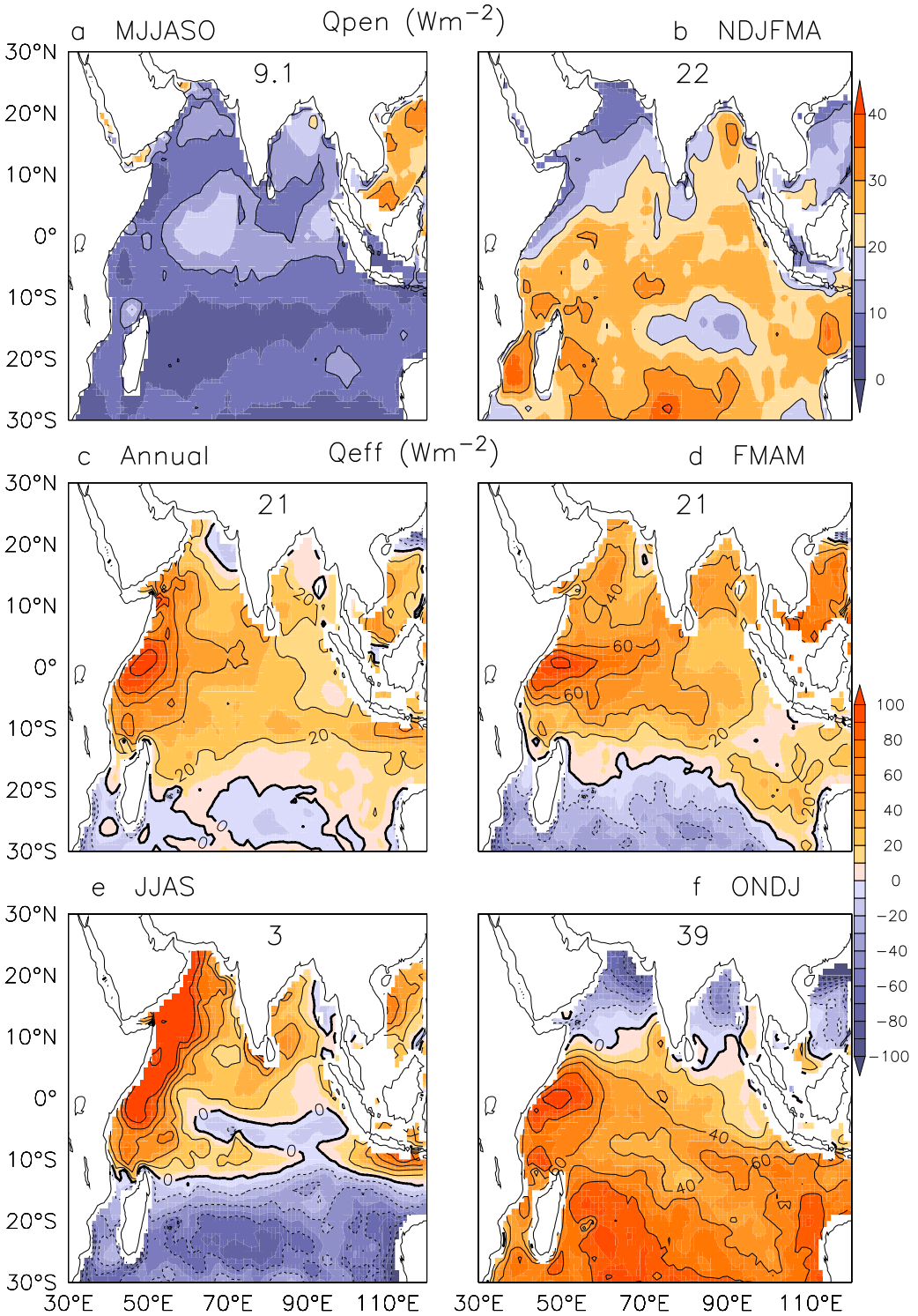

Figure 4. The 2003–2007 shortwave radiation penetrating below the mixed layer (Qpen; W m^{-2}) for (a) MJJASO and (b) NDJFMA; contour interval is 10 W m^{-2}. Effective heat flux (Qeff; W m^{-2}) 2003–2007, (c) annual mean, (d) FMAM, (e) JJAS, and (f) ONDJ; contour interval is 20 W m^{-2}. Basin-average values are mentioned in the plots.

radiation and latent heat flux are comparable, though the former is slightly higher, consistent with the findings of *Shinoda and Hendon* [1998] and *Schiller and Godfrey* [2003]. The variability of net longwave radiation is relatively small (Figure 5c), but a significant fraction of Qsw variability.

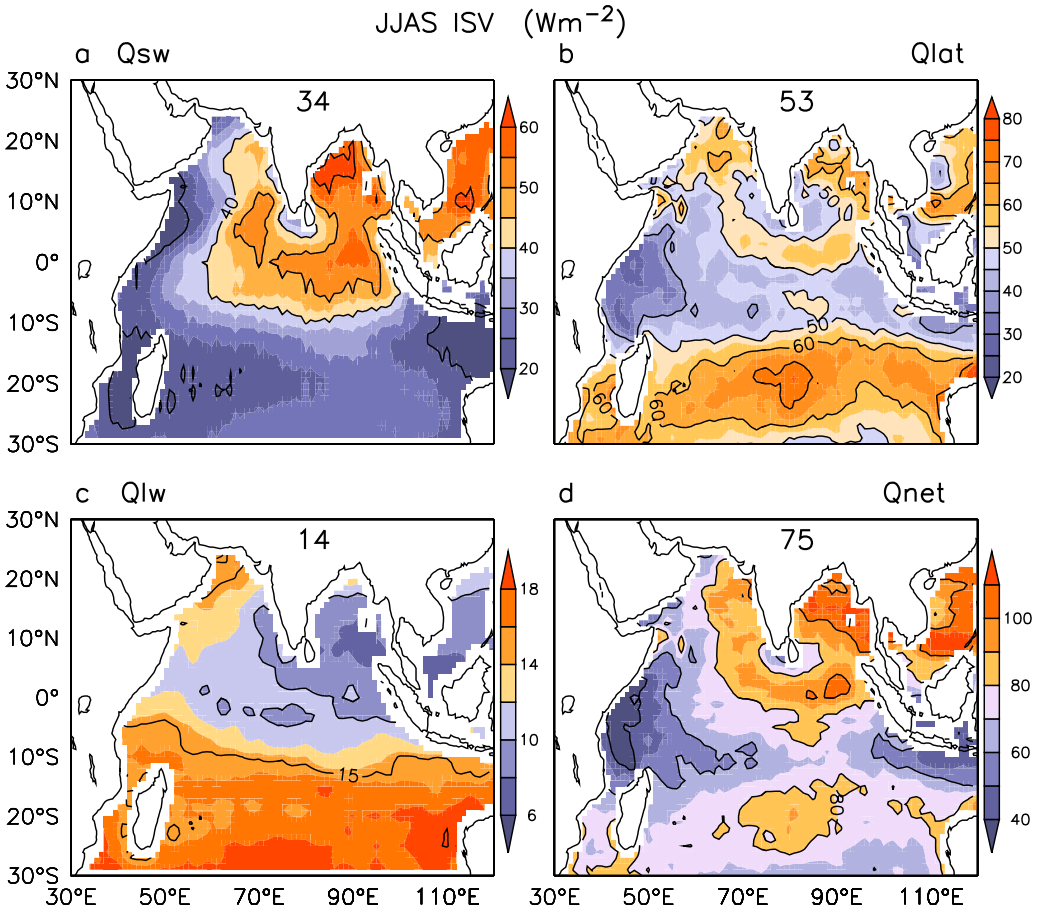

Figure 5. Standard deviation of subseasonal (2–90 day period) component of (a) net shortwave radiation (Qsw), (b) latent heat flux (Qlat), (c) net longwave radiation (Qlw), and (d) net heat flux (Qnet), in W m^{-2}. (a, b, d) The contour interval is 20 W m^{-2}, and (c) contour interval is 5 W m^{-2}.

The northward-propagating summer monsoon ISO and eastward-propagating MJO are mainly responsible for subseasonal variability of surface fluxes in the tropical Indian Ocean. The variability of organized tropical convection directly influences incident shortwave radiation [e.g., *Shinoda et al.*, 1998; *Sengupta et al.*, 2001], but is also closely related to variability of large-scale surface winds [e.g., *Zhang and McPhaden*, 2000]. We expect that variability of latent heat flux should depend on the combined effects of surface wind speed and near-surface specific humidity gradient. Evidence for modulation of surface humidity and air temperature by MJO or monsoon ISO has been limited by lack of reliable data with sufficient time resolution. *Tian et al.* [2006] used 2.5 years of AIRS air temperature and humidity to show that enhanced convection is preceded by a warm, moist anomaly in the lower atmosphere, and followed by a cool, dry anomaly in time (10 days) and space (30° longitude). They later confirmed these results using a longer stretch of AIRS data (7 years): Moist (dry) anomalies in the free troposphere (850–200 hPa) are associated with the convectively active (inactive) locations with peaks around 700 hPa [*Tian et al.*, 2010]. The availability of daily air temperature and specific humidity from the AIRS satellite product, calibrated against mooring data, allows us to estimate the contribution of Ta and Qa to the subseasonal variability of Qlat.

3.2.1. Sensitivity of Latent Heat Flux to Wind Speed, Air Temperature, Humidity, and SST

In order to quantify the relative contribution of wind speed, Ta and Qa to subseasonal variability (ISV for short) of latent heat flux, we artificially remove ISV from each of these fields, calculate the fluxes and examine the differences with the SatFlux "CONTROL" Qlat estimates. For instance, we estimate daily Qlat using seasonally varying wind speed (i.e., all variability with period less than 90 days is removed from the daily wind speed data), and call it the "No WIND ISV" experiment. Thus, any subseasonal variability of latent heat flux in the "No WIND ISV" experiment comes from subseasonal variability of Ta, Qa, and SST, but not wind speed. The daily root-mean-square difference (RMSD) between latent heat flux in the "CONTROL" and "No

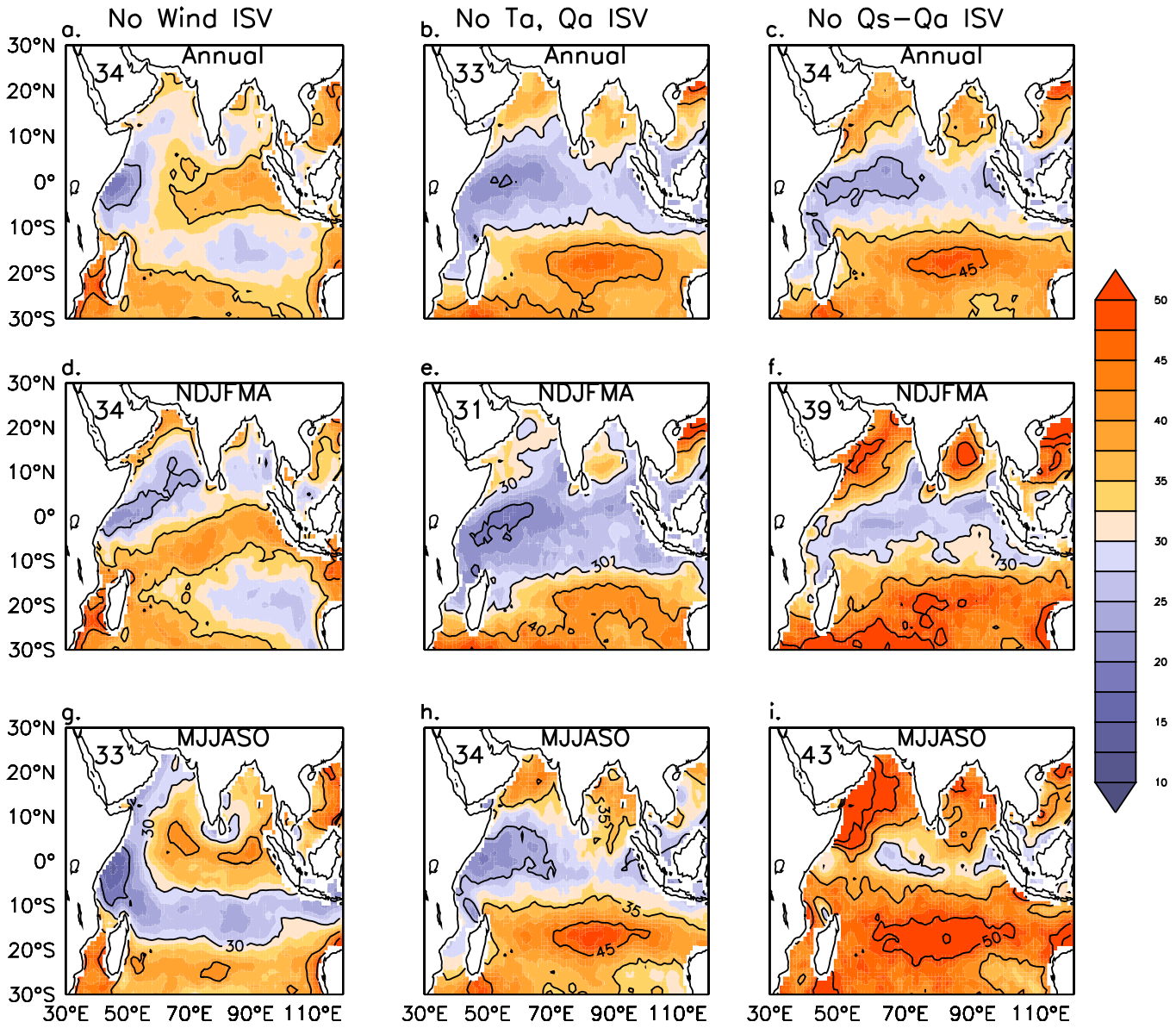

Figure 6. (a) Root-mean-square difference (RMSD) between "CONTROL" Qlat and "No Wind ISV" Qlat, 2003–2007 (W m^{-2}). As in Figure 6a, but for (d) austral summer NDJFMA and (g) boreal summer MJJASO. (b) As in Figure 6a, but for "No Ta, Qa ISV" Qlat; (e) NDJFMA and (h) MJJASO. (c) As in Figure 6a, but for "No (Qs-Qa) ISV" Qlat; (f) NDJFMA and (i) MJJASO.

WIND ISV" calculations represents the influence of wind speed variability. We do similar experiments by removing subseasonal variability from the SST field, both Ta and Qa fields, and both SST and Qa (called the "No Qa, Ta ISV," "No SST ISV," and "No (Qs-Qa) ISV" experiments). The year is divided into two seasons: boreal summer (MJJASO) and boreal winter (NDJFMA).

Figure 6 shows the contribution of wind ISV and Ta, Qa ISVs on the right. During NDJFMA, the largest effect of wind ISV (in excess of 35 W m^{-2}) lies in the central IO, south of the equator; this is broadly colocated with the tilted Inter Tropical Convergence Zone in winter (Figure 6c) [*Schott et al.*, 2009; *Xie et al.*, 2002]. During MJJASO, the impact of wind ISV is largest (>35 W m^{-2}) in the Bay of Bengal, equatorial IO and eastern Arabian Sea (Figure 6e). Thus, the maximum influence of wind ISV on Qlat appears to be broadly in the regions of organized convection (Figures 6c and 6e). In the No Ta, Qa ISV map, the striking feature is the low value (20–30 W m^{-2}) near the equator (10°S–10°N; Figure 6b). The spatial structure is similar in both seasons but magnitudes differ. In NDJFMA, the impact of Ta and Qa ISV exceeds 30 W m^{-2} in the Arabian Sea and Bay of Bengal, and 40 W m^{-2} off Australia (Figure 6d). During MJJASO, however, the values reach

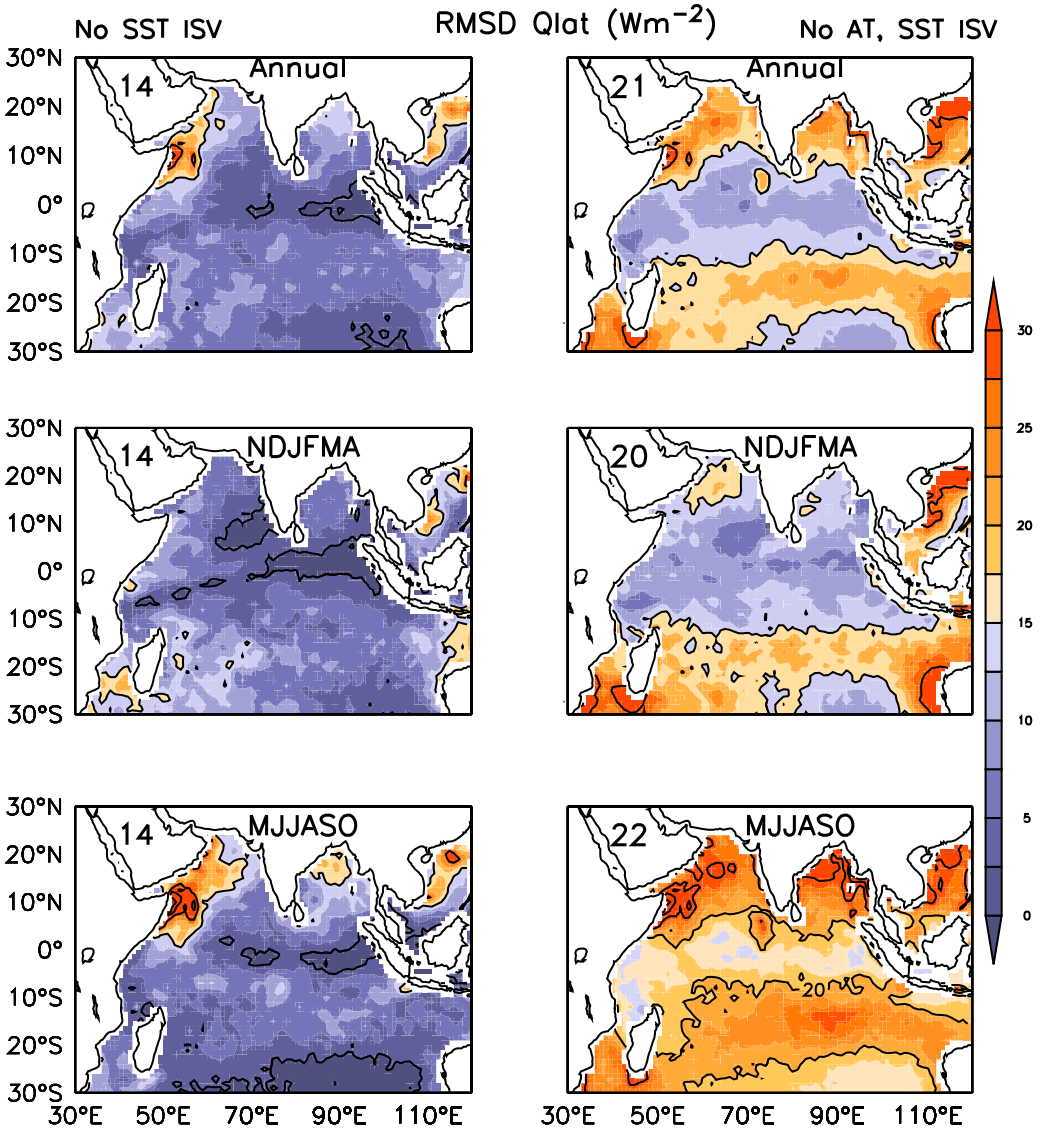

Figure 7. (a) Root-mean-square difference (RMSD) between "CONTROL" Qlat and "No SST ISV" Qlat, 2003–2007 (W m^{-2}). As in Figure 7a, but during (c) MJJASO and (e) NDJFMA. (b) As in Figure 7a, but for "No Ta, SST ISV" Qlat; (d) MJJASO and (f) NDJFMA.

60 W m^{-2} in the Arabian Sea and southern IO. Clearly, the influence of Ta and Qa ISV is modest near the equator but increases poleward (Figures 6d and 6f). We evaluate the influence of subseasonal variability of air-sea humidity difference on Qlat based on the "No (Qs-Qa) ISV" experiment. We find that the largest contribution of Qs-Qa ISV is away from the equator in both austral and boreal summer seasons NDJFMA and MJJASO (Figures 6f and 6i).

The basin-average contribution of wind ISV to Qlat is 34 W m^{-2} over the year, as well as in boreal winter and summer. The contribution of Ta and Qa ISVs to Qlat is 33 W m^{-2} annually (31 W m^{-2} in winter and 34 W m^{-2} in summer). Thus, on the subseasonal scales, Ta and Qa ISVs make significant contribution to Qlat, which is comparable to that of wind ISV; the contribution of air-sea humidity gradient to latent heat flux exceeds the contribution of wind speed variations. These are significant new results, because it is generally thought that latent heat flux variability, at least on annual or longer scales, is predominantly due to wind speed changes. We note that a couple of previous studies hint at a larger contribution of humidity: using numerical simulations *DeMott et al.* [2014] showed that near-surface vertical gradients of specific humidity and air-sea temperature contribute significantly to latent heat flux and are sensitive to SST variations in the Indian Ocean. *Zhou and Li* [2010] examined the upscale feedback of synoptic variability (3–8 days) to ISO

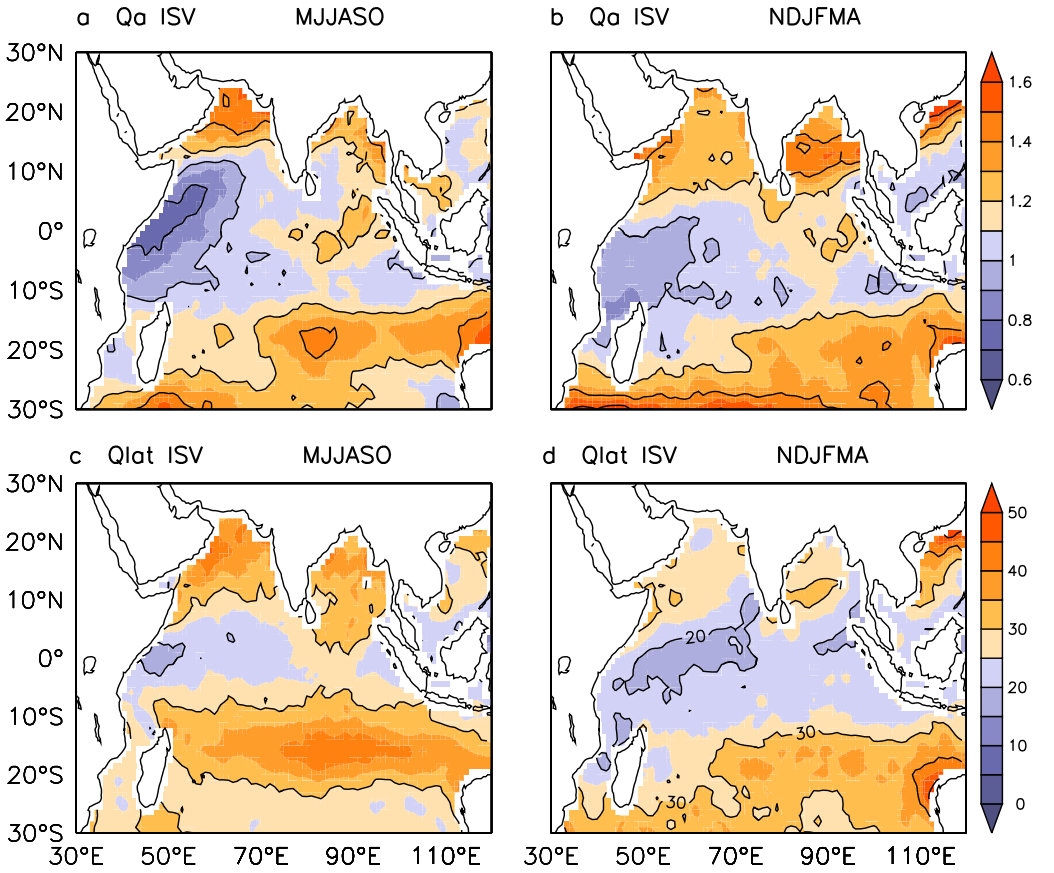

Figure 8. Subseasonal variability of Qa during (a) boreal summer (MJJASO) and (b) austral summer (NDJFMA) in g/kg. (c) Root-mean-square difference (RMSD) between "CONTROL" Qlat and "No Qa ISV" Qlat in W m^{-2} for MJJASO. (d) As in Figure 8c but for NDJFMA.

(20–90 days) via nonlinear rectification of Qlat. They report equal contributions of synoptic scale winds and (Qs-Qa) to intraseasonal Qlat.

For completeness, we show the sensitivity of Qlat to SST ISV and Ta ISV (Figure 7). In the first case, we suppress the ISVs in SST alone (Figure 7, left column); in the second, ISVs in both SST and Ta are suppressed (Figure 7, right column). The effect of the SST ISV on Qlat ISV is seen to be smaller in both seasons (14 W m^{-2}) compared to the combined effect of Ta and SST ISVs (about 20 W m^{-2}). Figure 8 shows the magnitude of specific humidity (Qa) ISV and contribution of Qa ISV to Qlat ISV during boreal summer (MJJASO) and boreal winter (NDJFMA). Qa ISV is high (>1.2 g/kg, Figure 8a) in the northern Arabian Sea and Bay of Bengal in MJJASO; Qlat ISV is also large in those regions, about 30 W m^{-2}, though the spatial extent is larger in the Bay of Bengal (Figure 8c). During NDJFMA, Qa ISV is large in the Arabian Sea and Bay of Bengal (Figure 8b) but the Qlat ISV is not very large (about 25 W m^{-2}, Figure 8d). The highest Qlat ISV during this season is seen south of 10°S, corresponding with the region of high Qa ISV.

3.3. Relation Between Subseasonal Variability of Fluxes and SST

The heat flux available to the ocean mixed layer (Qeff) along with ocean processes (mixing, advection, etc.) drive the rate of change of sea surface temperature ($^{\partial SST}/_{\partial t}$). Before we examine the relation between $^{\partial SST}/_{\partial t}$ and Qeff, we show the spatial patterns of subseasonal variability of SST and Qeff individually (Figure 9). In MJJASO, Qeff has largest ISV (>60 W m^{-2}) in the northern IO (Figure 9a) and in the southern IO (south of 20°S). The lowest ISV (<40 W m^{-2}) is in the western equatorial IO. During NDJFMA, the region of high ISV is the equatorial central and eastern IO (Figure 9a); ISV of Qeff is generally larger south of the equator in this season.

Summer SST ISV is higher than 0.3°C almost everywhere in the north IO, and relatively low south of the equator (Figure 9c). The most energetic SST ISV (0.5°C) occurs in the western Arabian Sea [*Vialard et al.*, 2010]. In boreal winter, low SST ISV (<0.3°C) is found in the northern and equatorial IO. Broadly speaking,

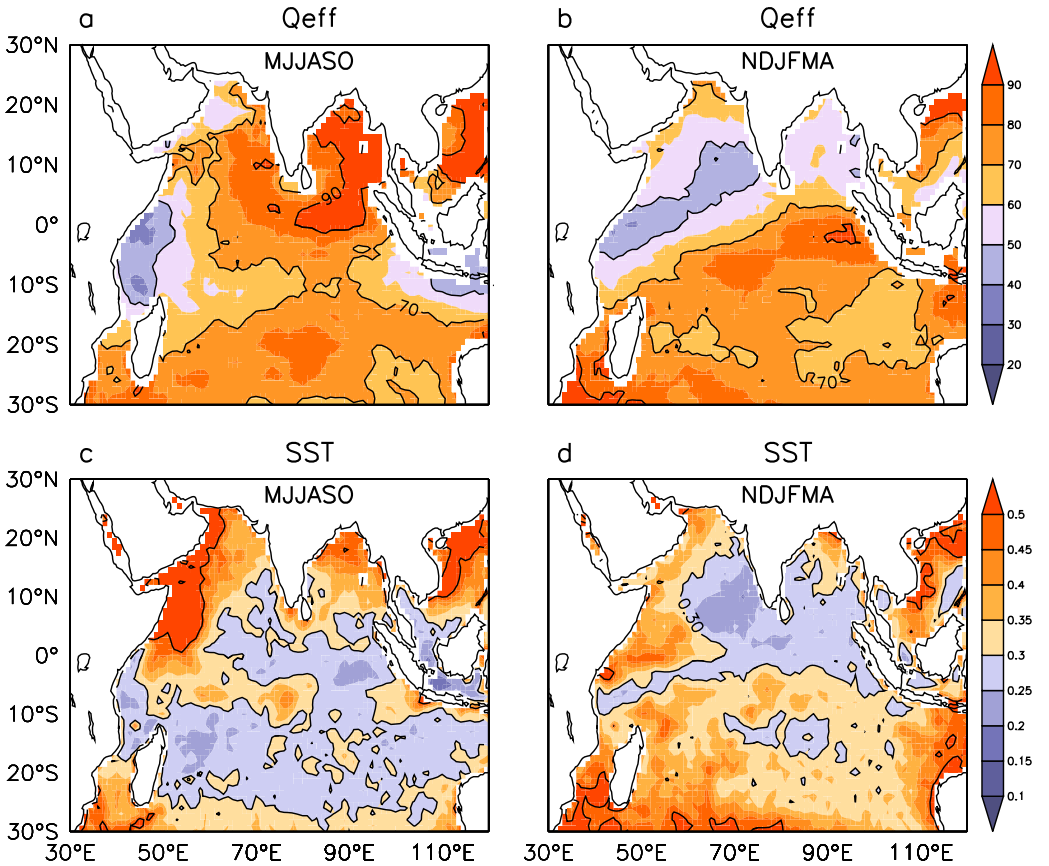

Figure 9. Subseasonal variability of Qeff (W m^{-2}) during (a) boreal summer (MJJASO) and (b) austral summer (NDJFMA). Subseasonal variability of SST (in °C) during (c) MJJASO and (d) NDJFMA.

both flux and SST have larger variability in the summer hemisphere, that is, in the north during MJJASO and in the south during NDJFMA.

In order to quantify the relation between Qeff and SST on subseasonal scales, we calculate the correlation coefficient (CC) between ISV of Qeff and $\rho.C_p.MLD.^{\partial SST}/_{\partial t}$ (hereafter $^{\partial SST}/_{\partial t}$ for brevity); a 10 day running mean is applied to suppress the very high frequencies. Another measure of the relation between heat flux and ocean response is "R," the ratio of the daily standard deviation (SD) of ($\rho.Cp.MLD.^{\partial SST}/_{\partial t}$) to SD of Qeff:

$$R = \frac{SD\left(\rho.Cp.MLD.\frac{\partial SST}{\partial t}\right)}{SD(Qeff)} \tag{6}$$

R is the ratio of SST variability to heat flux variability; when CC is close to 1 and R is close to 1, we say that subseasonal SST variability is mainly a response to Qeff. Figure 10 shows maps of R only in regions with CC of 0.4 or more; the regions in blue where R is close to one, denotes that Qeff is the main driver of SST variability. In regions where $R > 1$, the magnitude of SST variability is larger than that of Qeff, ocean processes act in phase with heat flux to warm or cool the ocean. In regions where $CC < 0.4$ we expect that SST variability is not mainly forced by heat flux; here ISV of SST must be primarily due to ocean processes (advection or entrainment/mixing).

Much of the north Indian Ocean shows high correlation (0.6 and above) between Qeff and $^{\partial SST}/_{\partial t}$ ISV during boreal summer (MJJASO; Figure 10a). Also note that the south-eastern Arabian Sea, Bay of Bengal, central and eastern equatorial Indian Ocean show R close to 1 (Figure 10c). This implies that heat flux is the dominant forcing of SST intraseasonal variability in the summer in the north Indian Ocean [*Sengupta et al.*, 2001; *Parampil et al.*, 2010]. In the northern Arabian Sea, CC is greater than 0.5 while $R > 1$, which implies that oceanic processes act in phase with heat fluxes to give a total SST "response" larger than heat flux forcing. The lowest (negative) correlations during MJJASO are found in the western Arabian Sea-western equatorial

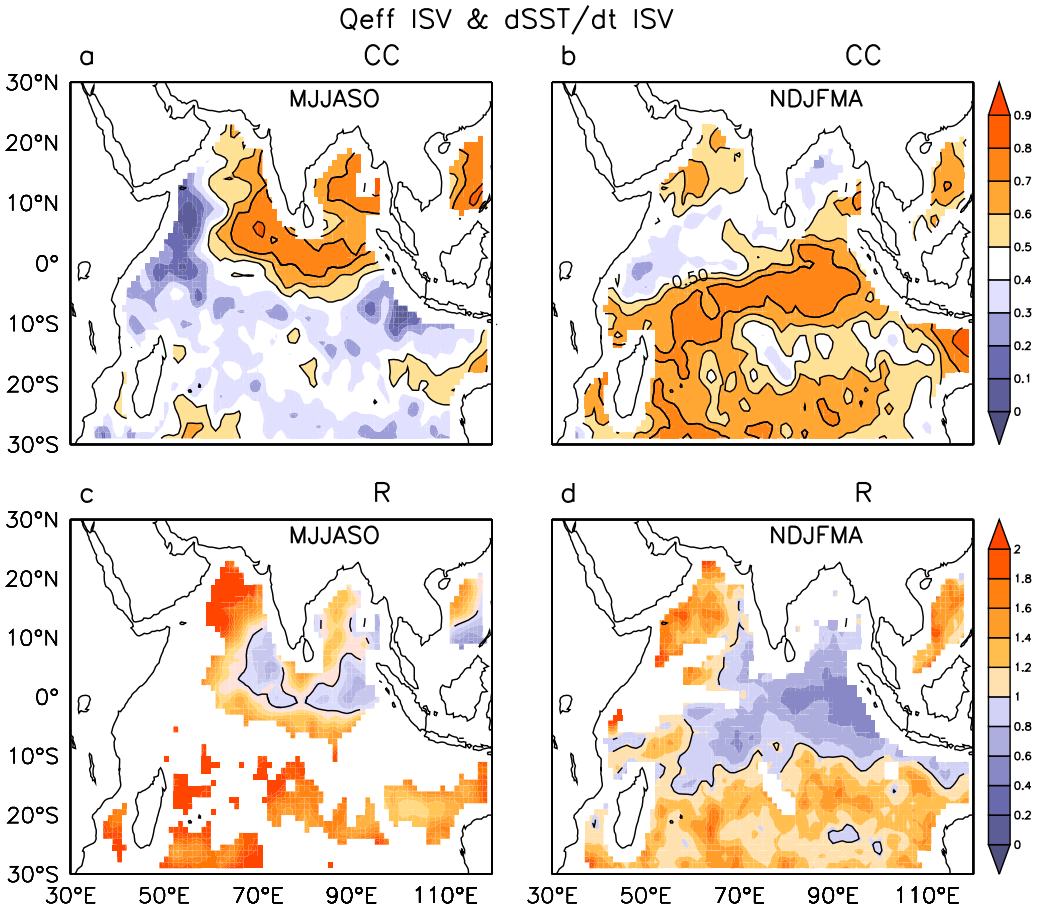

Figure 10. Correlation coefficient (CC) between subseasonal variability of Qeff and $^{\partial SST}/_{\partial t}$ during (a) boreal summer (MJJASO) and (b) austral summer (NDJFMA). CC is calculated from daily time series smoothed by a 10 day running average. R, the ratio of standard deviation of $^{\partial SST}/_{\partial t}$ ISV to Qeff ISV is shown for (c) MJJASO and (d) NDJFMA only in regions where CC exceeds 0.4.

Indian Ocean. During the southwest monsoon, the region is subject to wind-driven upwelling, resulting in cool SST. The presence of strong western boundary currents in the region gives rise to dynamic instabilities of different kinds. The strength of the upwelling as well as the instabilities can depend on the local and large-scale forcing by wind stress [*Schott and McCreary*, 2001]. The model experiments reported in *Vialard et al*. [2010] indicate that 30–90 day SST variability in this region is primarily due to wind stress variability and not heat flux. Hence on the seasonal [*Yu et al*., 2007] as well as intraseasonal time scales [*Vecchi et al*., 2004], ocean processes determine SST variability in the western Arabian Sea and western EqIO.

During austral summer (NDJFMA) the region of high correlation shifts to the southern hemisphere. Meanwhile, the northern hemisphere correlations are mostly between 0.5 and 0.3 (except in the western Arabian Sea). The highest correlations (0.5–0.7) are found in the thermocline ridge region (60°E–90°E, 5°S–10°S) [*Xie et al*., 2002] and the eastern equatorial Indian Ocean (Figure 10b). The response factor $R < 1$ over most of the thermocline ridge region. From November to April, the ITCZ is generally located south of the equator in the western Indian Ocean. As mentioned before, wind stress curl shoals the thermocline in the west via Ekman pumping. The ridge is shallowest in austral summer, and the mixed layer is thin, making it conducive to strong air-sea interaction such as those associated with the MJO. Consensus has yet to be reached on the reason for the large intraseasonal SST variability in the region; some attribute it to heat fluxes [*Vialard et al*., 2008; *Drushka et al*., 2012] while others emphasize the role of entrainment driven by wind stress [*Harrison and Vecchi*, 2001]; both fluxes and ocean processes are likely to be important [*Saji et al*., 2006; *Jayakumar et al*., 2010]. Our results suggest that heat flux drives SST variability in the region (Figures 10c and 10d); this is consistent with the findings of *Jayakumar et al*. [2010], who attribute 70% of SST variability to heat flux and about 20% to entrainment across the base of the mixed layer.

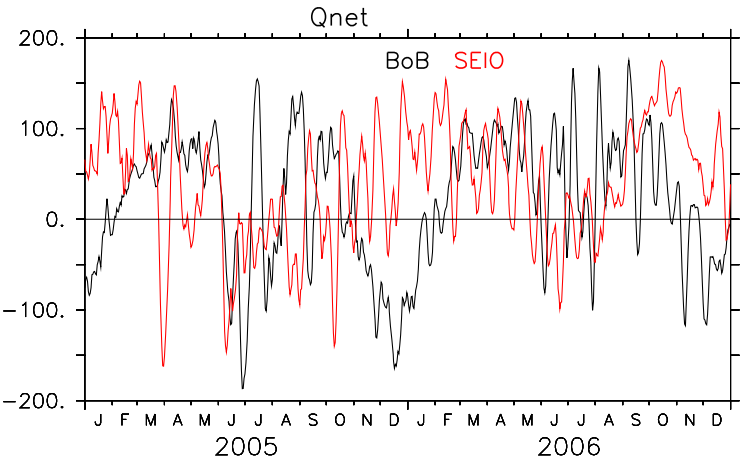

Figure 11. Time series of 7 day smoothed net heat flux Qnet (in W m^{-2}) in the northern Bay of Bengal (15°N–19°N, 86°E–90°E; black), and southeast Indian Ocean (6°S–10°S, 88°E–92°E; red).

Thus, our analysis suggests that subseasonal variability of heat flux determines subseasonal SST changes in the summer hemisphere, i.e., during May–October in the northern hemisphere and November–April in the southern hemisphere. It is important to note that the heat flux itself shifts between positive and negative throughout the year in the Indian Ocean (Figure 10). There are large positive and negative values of Qnet in the summer hemisphere i.e., during MJJASO in the Bay of Bengal and during NDJFMA in the Southeast Indian Ocean (Figure 11). When the heat flux is positive it warms the ocean and when negative it cools the ocean even without ocean processes. The heat flux variability in the summer hemisphere is associated with organized convection (monsoon ISO or MJO): during periods of active convection, cloudy skies (low Qsw) and strong winds (high Qlat) lead to negative Qnet while suppressed convection (clear skies and weak winds) lead to positive Qnet.

4. Conclusions

We have used satellite observations and a ship-based climatology to construct an experimental data set on daily radiative and turbulent heat fluxes over the Indian Ocean for the period 2003–2007. The novelty of our approach is the use of daily satellite air temperature and humidity calibrated against buoy data. Comparison with buoy estimates shows that our observation-based fluxes capture subseasonal variability of heat flux with reasonable accuracy.

On subseasonal time scales, we find the largest amplitude of heat flux variability (80 W m^{-2}) during boreal summer. Subseasonal Qsw and Qlat associated with organized convection combine to give large variability in Qnet [e.g., *Sengupta and Ravichandran*, 2001]. Over the tropical Indian Ocean, the combined variability of air temperature and humidity contributes as much as wind variability to Qlat ISV, and subseasonal variability of near-surface humidity gradient contributes significantly more than variability of surface wind speed (Figure 6). The effect of subseasonal variability of air temperature and humidity on Qlat is enhanced away from the equator (Figures 6 and 8). This is mainly because air temperature and humidity themselves have large variability near land and in the southern IO (30°S–15°S). The large ISV in air temperature, humidity and Qlat are possibly enhanced by wind blowing off the Asian and Australian continents, but other factors related to time-varying subsidence, or downdrafts bringing cool, dry air to the surface, could be important too. We note that the subseasonal variability of latent heat flux in our flux product is somewhat larger than in OAFlux or TropFlux, at least in the equatorial Indian Ocean (supporting information Figure S6).

We have presented unified results on the relation between ISV of Qeff and SST in the entire tropical IO in two seasons (boreal summer MJJASO and austral summer NDJFMA). The results are based on about 900 days of data for each season, so that the number of degrees of freedom is reasonably large. The largest intraseasonal variability is over the northeast Indian Ocean during MJJASO and over the southern Indian Ocean (15°S–equator) and the eastern equatorial IO during NDJFMA. The regions of high correlation (>0.5) between Qeff and $^{\partial SST}/_{\partial t}$, and $R < 1$ lie in the northeast Indian Ocean during MJJASO, the thermocline ridge region and the eastern equatorial Indian Ocean during NDJFMA. The implication is that SST responds to intraseasonal heat flux variations in regions of large-scale organized convection in the summer hemisphere. This result goes beyond most previous studies, which use filtered data and focus on either monsoon ISO in boreal summer or MJO in boreal winter [e.g., see *Lau and Waliser*, 2012]. Based on this result, we propose

that subseasonal variability of SST is coherent with flux variability not just because ocean temperature responds to heat flux, but because the SST field plays an active role in the organization and movement of tropical deep convection in the summer hemisphere.

Acknowledgments
The authors gratefully acknowledge the Ministry of Earth Sciences, New Delhi, for funding this research under the INDOMOD and Monsoon Mission OMM programmes. Thanks are due to Jerome Vialard and Matthieu Lengaigne for useful discussions on the satellite-based flux project. We also gratefully acknowledge the development teams and agencies for the following data sets: Dasilva94, ISCCP (ftp://isccp.giss.nasa.gov/outgoing/FLUX/SRF.), RAMA and TAO mooring data, TMI-AMSRE (ftp://ftp.discover-earth.org/sst/daily/tmiamsre.), QSCATFSU (http://coaps.fsu.edu/scatterometry/gridded/), SeaWIFS monthly chlorophyll *a*, NOCS, OAFLUX, and TropFLUX. The AIRS data used in this study were acquired as part of the NASA's Earth-Sun System Division and archived and distributed by the Goddard Earth Sciences (GES) Data and Information Services Center (DISC) Distributed Active Archive Center (DAAC). AIRS is available at http://apdrc.soest.hawaii.edu/data/data.php.

References

Achuthavarier, D., and V. Krishnamurthy (2011), Role of Indian and Pacific SST in Indian summer monsoon intraseasonal variability, *J. Clim.*, *24*, 2915–2930, doi:10.1175/2010JCLI3639.1.

Bellenger, H., and J. P. Duvel (2007), Intraseasonal convective perturbations related to the seasonal march of the Indo-Pacific Monsoons, *J. Clim.*, *20*, 2853–2863, doi:10.1175/JCLI4182.1.

Conkright, M. E., et al. (2002), World Ocean Database 2001, vol. 1, Introduction, NOAA Atlas NESDIS 42 [CD-ROM], edited by S. Levitus, 167 pp., U.S. Govt. Print. Off., Washington, D. C.

da Silva, A. M., C. C. Young, and S. Levitus (1994), *Atlas of Surface Marine Data 1994*, vol. 4, Anomalies of fresh water fluxes, NOAA Atlas, NESDIS, 9.

de Boyer Montegut, C., G. Madec, A. S. Fischer, A. Lazar, and D. Iudicone (2004), Mixed layer depth over the global ocean: An examination of profile data and a profile-based climatology, *J. Geophys. Res.*, *109*, C12003, doi:10.1029/2004JC002378.

DeMott, C. A., C. Stan, D. A. Randall, J. L. Kinter, and M. Khairoutdinov (2011), The Asian monsoon in the superparameterized CCSM and its relationship to tropical wave activity, *J. Clim.*, *24*, 5134–5156, doi:10.1175/2011JCLI4202.1.

DeMott, C. A., C. Stan, D. A. Randall, and M. D. Branson (2014), Intraseasonal variability in coupled GCMs: The roles of ocean feedbacks and model physics, *J. Clim.*, *27*, 4970–4995, doi:10.1175/JCLI-D-13-00760.1.

Drushka, K., J. Sprintall, S. T. Gille, and S. Wijffels (2012), In site observations of Madden-Julian Oscillation mixed layer dynamics in the Indian and Western Pacific Oceans, *J. Clim.*, *25*, 2306–2328, doi:10.1175/JCLI-D-11-00203.1.

Duvel, J. P., and J. Vialard (2007), Indo-Pacific sea surface temperature perturbations associated with intraseasonal oscillations of tropical convection, *J. Clim.*, *20*, 3056–3082, doi:10.1175/JCLI4144.1.

Fu, X., B. Wang, T. Li, and J. P. McCreary (2003), Coupling between northward-propagating, intraseasonal oscillations and sea surface temperature in the Indian Ocean, *J. Atmos. Sci.*, *60*, 1733–1753, doi:10.1175/15200469(2003)060<1733:CBNIOA>2.0.CO;2.

Gentemann, C. L., F. J. Wentz, C. A. Mears, and D. K. Smith (2004), In situ validation of tropical rainfall measuring mission microwave sea surface temperatures, *J. Geophys. Res.*, *109*, C04021, doi:10.1029/2003JC002092.

Goswami, B. N. (2012), *South Asian Monsoon, Intraseasonal Variability in the Atmosphere-Ocean Climate System*, edited by W. K. M. Lau and D. Waliser, pp. 21–72, Springer, Berlin Heidelberg.

Halkides, D. J., D. E. Waliser, T. Lee, D. Menemenlis, and B. Guan (2015), Quantifying the processes controlling intraseasonal mixed layer temperature variability in the tropical Indian Ocean, *J. Geophys. Res. Oceans*, *120*, 692–715, doi:10.1002/2014JC010139.

Han, W., W. T. Liu, and J. Lin (2006), Impact of atmospheric submonthly oscillations on sea surface temperature of the tropical Indian Ocean, *Geophys. Res. Lett.*, *33*, L03609, doi:10.1029/2005GL025082.

Harrison, D. E., and G. A. Vecchi (2001), January 1999 Indian ocean cooling event, *Geophys. Res. Lett.*, *28*, 3717–3720, doi:10.1029/2001GL013506.

Jayakumar, A., J. Vialard, M. Lengaigne, C. Gnanaseelan, J. P. McCreary, and B. Praveenkumar (2010), Processes controlling the surface temperature signature of the Madden-Julian oscillation in the thermocline ridge of the Indian Ocean, *Clim. Dyn.*, *37*(11), 2217–2234, doi:10.1007/s00382 010-0953-5.

Josey, J. A., E. C. Kent, and P. K. Taylor (1999), New insights into the ocean heat budget closure problem from analysis of the SOC air sea flux climatology, *J. Clim.*, *12*, 2856–2880, doi:10.1175/1520-0442(1999)012≤2856:NIITOH≥2.0.CO;2.

Kalnay, E., et al. (1996), The NCEP/NCAR 40-year reanalysis project, *Bull. Am. Meteorol. Soc.*, *77*, 437–471.

Lau, W. K. M., and D. E. Waliser (Eds.) (2012), *Intraseasonal Variability in the Atmosphere-Ocean Climate System*, 2nd ed., Springer.

Liu, W. T. (2002), Progress in scatterometer application, *J. Oceanogr.*, *58*, 121–136, doi:10.1023/A:1015832919110.

Lloyd, I., and G. A. Vecchi (2010), Submonthly Indian ocean cooling events and their interaction with large-scale conditions, *J. Clim.*, *23*, 700–716, doi:10.1175/2009JCLI3067.1.

Manizza, M., C. L. Quere, A. J. Watson, and E. T. Buitenhuis (2005), Bio-optical feedbacks among phytoplankton, upper ocean physics and sea-ice in a global model, *Geophys. Res. Lett.*, *32*, L05603, doi:10.1029/2004GL020778.

McPhaden, M. J., et al. (1998), The tropical ocean-global atmosphere (TOGA) observing system: A decade of progress, *J. Geophys. Res.*, *103*, 14,169–14,240, doi:10.1029/97JC02906.

McPhaden, M. J., G. Meyers, K. Ando, Y. Masumoto, V. S. N. Murty, M. Ravichandran, F. Syamsudin, J. Vialard, L. Yu, and W. Yu (2009), RAMA: The research moored array for African-Asian-Australian Monsoon Analysis and prediction, *Bull. Am. Meteorol. Soc.*, *90*, 459–480, doi:10.1175/2008BAMS2608.

Morel, A., and D. Antoine (1994), Heating rate within the upper ocean in relation to its bio-optical state, *J. Phys. Oceanol.*, *24*, 1652–1665, doi:10.1175/1520-0485(1994)024 <1652:HRWTUO>2.0.CO;2.

Murtugudde, R., and A. J. Busalacchi (1999), Interannual variability of the dynamics and thermodynamics of the tropical Indian Ocean, *J. Clim.*, *12*, 2300–2326, doi:10.1175/1520-0442(1999)012 < 2300:IVOTDA>2.0.CO;2.

Olsen, E. T., et al. (2007), AIRS/AMSU/HSB Version 5 data release user guide, Jet Propulsion Laboratory, California Institute of Technology, Pasadena, Calif. [Available at http://disc.sci.gsfc.nasa.gov/AIRS/documentation/v5_docs.]

Olsen, E. T., et al. (2013), AIRS/AMSU/HSB Version 6 Changes from Version 5, Jet Propulsion Laboratory, California Institute of Technology, Pasadena, Calif. [Available at http://disc.sci.gsfc.nasa.gov/AIRS/documentation/v6_docs/v6releasedocs-1/V6_Changes_from_V5.pdf.]

Parampil, S. R., A. Gera, M. Ravichandran, and D. Sengupta (2010), Intraseasonal response of mixed layer temperature and salinity in the Bay of Bengal to heat and freshwater flux, *J. Geophys. Res.*, *115*, C05002, doi:10.1029/2009JC005790.

Paulson, C. A., and J. J. Simpson (1977), Irradiance measurements in the upper ocean, *J. Phys. Oceanogr.*, *7*, 952–956, doi:10.1175/1520-0485(1977)007 < 0952:IMITUO>2.0.CO;2.

Pegion, P. J., M. A. Bourassa, D. M. Legler, and J. J. O'Brien (2000), Objectively-derived daily 'winds' from satellite scatterometer data, *Mon. Weather Rev.*, *128*, 3150–3168, doi:10.1175/1520-0493(2000)128<3150:ODDWFS>2.0.CO;2.

Pradhan, Y., M. Mohan, D. Sengupta, and S. Nayak (2005), Radiant heating rates and surface biology during the Arabian Sea monsoon experiment, *J. Geophys. Eng.*, *2*, 16–22.

Praveenkumar, B., J. Vialard, M. Lengaigne, V. S. N. Murty, and M. J. McPhaden (2011), TropFlux: Air-sea fluxes for the global tropical oceans—Description and evaluation against observations, *Clim. Dyn.*, *38*, 1521–1543, doi:10.1007/s00382-011-1115-0.

R. R. Rao, and R. Sivakumar (2003), Seasonal variability of sea surface salinity and salt budget of the mixed layer of the north Indian Ocean, *J. Geophys. Res.*, *108*(C1), 3009, doi:10.1029/2001JC000907.
Rossow, W. B., and Y. C. Zhang (1995), Calculation of surface and top of atmosphere radiative fluxes from physical quantities based on ISCCP data sets 2. Validation and first results, *J. Geophys. Res.*, *100*, 1167–1197, doi:10.1029/94JD02746.
Roxy, M., and Y. Tanimoto (2007), Role of SST over the Indian ocean in influencing the intraseasonal variability of the Indian summer monsoon, *J. Meteorol. Soc. Jpn.*, *85*, 349–358, doi:10.2151/jmsj.85.349.
Saji, N. H., S. P. Xie, and C. Y. Tam (2006), Satellite observations of intense intraseasonal cooling events in the tropical south Indian Ocean, *Geophys. Res. Lett.*, *33*, L14704, doi:10.1029/2006GL026525.
Schiller, A., and J. S. Godfrey (2003), Indian Ocean intraseasonal variability in a ocean general circulation model, *J. Clim.*, *10*, 465–472, doi:10.1175/1520-0442(2003)016 < 0021:IOIVIA>2.0.CO;2.
Schiller, A., and P. R. Oke (2015), Dynamics of ocean surface mixed layer variability in the Indian Ocean, *J. Geophys. Res. Oceans*, *120*, 4162–4186, doi:10.1002/2014JC010538.
Schott, F., and J. P. McCreary (2001), The monsoon circulation of the Indian Ocean, *Prog. Oceanogr.*, *51*, 1–123, doi:10.1016/S0079-6611(01)00083-0.
Schott, F., S. P. Xie, and J. P. McCreary (2009), The monsoon circulation of the Indian Ocean, *Rev. Geophys.*, *47*, 1–46, doi:10.1029/2007RG000245.
Sengupta, D., and M. Ravichandran (2001), Oscillations of Bay of Bengal sea surface temperature during the 1998 summer monsoon, *Geophys. Res. Lett.*, *28*, 2033–2036, doi:10.1029/2000GL012548.
Sengupta, D., B. N. Goswami, and R. Senan (2001), Coherent intraseasonal oscillations of ocean and atmosphere during the Asian summer monsoon, *Geophys. Res. Lett.*, *28*, 21, 4127–4130, doi:10.1029/2001GL013587.
Sharmila, S., P. A. Pillai, S. Joseph, M. Roxy, R. P. M. Krishna, R. Chattopadhyay, S. Abhilash, A. K. Sahai, and B. N. Goswami (2013), Role of ocean-atmosphere interaction on northward propagation of Indian summer monsoon intraseasonal oscillation (MISO), *Clim. Dyn.*, *41*, 1651–1669, doi:10.1007/s00382-013-1854-1.
Shinoda, T., and H. Hendon (1998), Mixed layer modeling of intraseasonal variability in the tropical western Pacific and Indian oceans, *J. Clim.*, *11*, 2668–2685, doi:10.1175/1520-0442(1998)011<2668:MLMOIV>2.0.CO;2.
Shinoda, T., H. H. Hendon, and J. Glick (1998), Intraseasonal variability of surface fluxes and sea surface temperature in the tropical western Pacific and Indian oceans, *J. Clim.*, *11*, 1685–1702, doi:10.1175/1520-0442(1998)011<1685:IVOSFA>2.0.CO;2.
Sobel, A. H., E. D. Maloney, G. Bellon, and D. M. Frierson (2010), Surface Fluxes and Tropical Intraseasonal Variability: A Reassessment, *J. Adv. Model. Earth Syst.*, *2*, 2, doi:10.3894/JAMES.2010.2.2.
Tian, B., D. E. Waliser, E. J. Fetzer, B. H. Lambrigtsen, Y. L. Yung, and B. Wang (2006), Vertical moist thermodynamic structure and spatial–temporal evolution of the MJO in AIRS observations, *J. Atmos. Sci.*, *63*, 2462–2485, doi:10.1175/JAS3782.1.
Tian, B., D. E. Waliser, E. J. Fetzer, and Y. L. Yung (2010), Vertical moist thermodynamic structure of the Madden–Julian Oscillation in atmospheric infrared sounder retrievals: An update and a comparison to ECMWF interim re-analysis, *Mon. Weather Rev.*, *138*, 4576–4582, doi:10.1175/2010MWR3486.1.
Vecchi, G. A., and D. E. Harrison (2002), Monsoon breaks and subseasonal sea surface temperature variability in the Bay of Bengal, *J. Clim.*, *15*, 1485–1493, doi:10.1175/1520-0442(2002)015 <1485:MBASSS>2.0.CO;2.
Vecchi, G. A., S. P. Xie, and A. Fischer (2004), Ocean-atmosphere covariability in the western Arabian sea, *J. Clim.*, *17*, 1213–1224, doi:10.1175/1520-0442(2004)017 < 1213:OCITWA>2.0.CO;2.
Vialard, J., G. Foltz, M. McPhaden, J. P. Duvel, and C. de Boyer Montegut (2008), Strong Indian ocean sea surface temperature signals associated with the Madden-Julian oscillation in late 2007 and early 2008, *Geophys. Res. Lett.*, *35*, L19608, doi:10.1029/2008GL035238.
Vialard, J., A. Jayakumar, C. Gnanaseelan, M. Lengaigne, D. Sengupta, and B. N. Goswami (2010), Processes of 30-90 days sea surface temperature variability in the northern Indian Ocean during boreal summer, *Clim. Dyn.*, *90*, 45–61, doi:10.1007/s00382-011-1015-3.
Vinayachandran, P. N., and N. H. Saji (2008), Mechanisms of south Indian Ocean intraseasonal cooling, *Geophys. Res. Lett.*, *35*, L23607, doi:10.1029/2008GL035733.
Waliser, D. E., R. Murtugudde, and L. E. Lucas (2004), Indo-Pacific ocean response to atmospheric intraseasonal variability: 2. Boreal summer and the intraseasonal oscillation, *J. Clim.*, *109*, C03030, doi:10.1029/2003JC002002.
Weller, R. A., M. F. Baumgartner, S. A. Josey, A. S. Fischer, and J. C. Kindle (1998), Atmospheric forcing in the Arabian Sea during 1994-1995: Observations and comparisons with climatology and models, *Deep Sea Res., Part II*, *45*, 1961–1999, doi:10.1016/S0967-0645(98)00060-5.
WOCE Data Products Committee (2002), WOCE Global Data, version 3.0, Rep. 180/02, WOCE Int. Project Off., Southampton, U. K.
Xie, S. P., H. Annamalai, F. Schott, and J. P. McCreary (2002), Origin and predictability of south Indian Ocean climate variability, *J. Clim.*, *15*, 864–874, doi:10.1175/1520-0442(2002)015 < 0864:SAMOSI>2.0.CO;2.
Yu, L., and R. A. Weller (2007), Objectively analyzed air-sea heat fluxes for the global ice-free oceans, Bull. *Am. Meteorol. Soc.*, *88*, 527–539, doi:10.1175/BAMS-88-4-527.
Yu, L., X. Jin, and R. A. Weller (2007), Annual, seasonal, and interannual variability of air-sea heat fluxes in the Indian Ocean, *J. Clim.*, *20*, 3190–3209, doi:10.1175/JCLI4163.1.
Zeng, X., M. Zhao, and R. E. Dickinson (1998), Intercomparison of bulk aerodynamic algorithms for the computation of sea surface fluxes using TOGA COARE and TAO data, *J. Clim.*, *11*, 2628–2644, doi:10.1175/1520-0442(1998)011<2628:IOBAAF>2.0.CO;2.
Zhang, C., and M. J. McPhaden (2000), Intraseasonal surface cooling in the equatorial western Pacific, *J. Clim.*, *13*, 2261–2276, doi:10.1175/1520-0442(2000)013 < 2261:ISCITE>2.0.CO;2.
Zhang, Y., W. B. Rossow, A. A. Lacis, V. Oinas, and M. I. Mishchenko (2004), Calculation of radiative fluxes from the surface to top of atmosphere based on ISCCP and other global data sets: Refinements of the radiative transfer model and the input data, *J. Geophys. Res.*, *109*, D19105, doi:10.1029/2003JD004457.
Zheng, Y., D. E. Waliser, W. F. Stern, and C. Jones (2004), The role of coupled sea surface temperatures in the simulation of the tropical intraseasonal oscillation, *J. Clim.*, *17*, 4109–4134, doi:10.1175/JCLI3202.1.
Zhou, C., and T. Li (2010), Upscale feedback of tropical synoptic variability to intraseasonal oscillations through the nonlinear rectification of the surface latent heat flux, *J. Clim.*, *23*, 5738–5754, doi:10.1175/2010JCLI3468.1.
Zhou, L., R. Murtugudde, and M. Jochum (2008), Dynamics of the intraseasonal oscillations in the Indian Ocean south equatorial current, *J. Phys. Oceanogr.*, *38*, 121–132, doi:10.1175/2007JPO3730.1.p